Supplementary Information

Phosphorus doped molybdenum disulfide regulated by sodium chloride for advanced supercapacitor electrode

Yunan Li,[*ab] Jiayin Meng,[a] Xiaotian Wang,[a] Meng Song,[a] Mingli Jiao,[a] Qi Qin,[*a] Liwei Mi[*b]

[a]School of Materials and Chemical Engineering, Zhongyuan University of Technology, Zhengzhou 450007, China

[b]Center for Advanced Materials Research, Henan Key Laboratory of Functional Salt Materials, Zhongyuan University of Technology, Zhengzhou 450007, China

* Corresponding authors.

E-mail addresses: yunanli@zut.edu.cn (Y. Li), qq@zut.edu.cn (Q. Qin), mlwzzu@163.com (L. Mi).

1. Experimental

1.1. Preparation of phosphorus doped molybdenum disulfide regulated by sodium chloride (SP-MoS_2)

SP-MoS_2 was prepared by one-step hydrothermal reaction. In a typical procedure, 0.58 mmol phosphomolybdate acid (PMo_{12}) was added into 15 mL deionized water and stirred for 0.5 h, denoted as solution A. 15 mmol thiourea ($(NH_2)_2CS$) and 0.5 g sodium chloride (NaCl) were added into 15 mL of deionized water and stirred for 0.5 h, denoted as solution B. The solution A was mixed with solution B under stirring. The mixed solution was then transferred into a 50 mL Teflon-lined stainless-steel autoclave and kept at 180 °C for 24 h. After cooled down naturally to room temperature, the resultant precipitate was collected by centrifugation, washed with water and absolute ethanol several times, respectively, and finally dried at 60 °C overnight. Keeping other reaction conditions unchanged, when the amount of NaCl added was respectively 0.25 g, 0.75 g, and 0 g, the obtained sample was denoted as SP-MoS_2-0.25, SP-MoS_2-0.75 and P-MoS_2, respectively. MoS_2 was prepared when ammonium molybdate tetrahydrate (1 mmol) and thiourea (15 mmol) were used as starting materials and without addition of NaCl.

1.2. Characterization

The morphologies of the samples were examined by a scanning electron microscope (SEM, ZEISS Sigma 300) and a transmission electron microscope (TEM, JEOL JEM-F200). The structure of the samples was studied by an X-ray diffractometer (XRD; Ultima-IV) with Cu Kα radiation (λ = 0.15141 nm). X-ray photoelectron spectroscopy (XPS, Thermo Scientific K-Alpha) was measured with a monochromatic Al Kα X-ray source (hv = 1486.6 eV). The specific surface area and pore size distribution was derived from nitrogen adsorption/desorption isotherms (Micromeritics ASAP 2460) at 77 K using the Brunauer-Emmett-Teller (BET) method and Barrett-Joyner-Halenda (BJH) model, respectively.

1.3. Electrochemical measurements

All the electrochemical tests were carried out using 2 M KOH as the electrolyte. The working electrode was prepared by mixing the obtained sample as the active material, polyvinylidene fluoride as the binder and acetylene black as the conductive agent with a weight ratio of 8:1:1 in N-methyl-2-pyrrolidone solvent. Then the slurry was spread on foam nickel, dried overnight at the temperature of 80 ^{o}C. Finally, a 10 MPa pressure was applied on the electrode. The active material mass for each electrode was about 2~3 mg cm^{-2}. For three-electrode system, Pt foil and Hg/HgO electrode was used as the counter electrode and the reference electrode, respectively. A two-electrode system was utilized to investigated the electrochemical behavior of ASC. To assemble the ASC device, SP-MoS_2 and AC was used as positive electrode and negative electrode, respectively.

Cyclic voltammetry (CV), galvanostatic charge-discharge (GCD) and electrochemical impedance spectroscopy (EIS, frequency: 0.1 Hz–100 kHz) curves were obtained by using a CHI 660E electrochemical workstation at room temperature. The specific capacitance was calculated according to the GCD curves by using the equation 1:

$$C = \frac{I\Delta t}{m\Delta V} \tag{1}$$

Where C represents the specific capacitance (F g^{-1}), I (A) refers to the discharge current, ΔV (V) represents the potential change within the discharge time Δt (s), m (g) corresponds to the mass of active material in three-electrode system and total mass of active material in two-electrode system.

The energy density E (W h kg^{-1}) and power density P (W kg^{-1}) of the ASC device in two-electrode were calculated according to equations 2 and 3:

$$E = \frac{1}{2}C\Delta V^2 \times \frac{1}{3.6} \tag{2}$$

$$P = \frac{3600E}{\Delta t} \tag{3}$$

Where C (F g^{-1}) is the specific capacitance of the ASC device, ΔV (V) represents the potential change within the discharge time Δt (s).

1.4. Computational methodology

All first-principles calculations were performed based on density functional theory (DFT) using the Cambridge Sequential Total Energy Package (CASTEP).[1] The generalized gradient approximation (GGA)[2] with the Perdew-Burke-Ernzerhof (PBE) formula[3] were used for the exchange-correlation potential in combination with the DFT-D correction. The Broyden-Fletcher-Goldfarb-Shanno (BFGS) method was used to search for the ground state of the supercells, and the convergence tolerance was set to the energy change below 10^{-5} eV per atom, force less than 0.02 eV $Å^{-1}$, stress less than 0.05 GPa and displacement change less than 0.001 Å. The cutoff energy of the atomic wave functions was set to 450 eV.

The adsorption energy (E_{ads}) can be obtained by using the equation 4:

$$E_{ads} = E_{substrate/adsorbate} - E_{substrate} - E_{adsorbate} \quad (4)$$

Where $E_{substrate/adsorbate}$ is the total energy of the complex formed by substrate interacting with adsorbates, $E_{substrate}$ is the energy of the substrate, and $E_{adsorbate}$ is the energy of the isolated adsorbate.[4, 5]

2. Figures

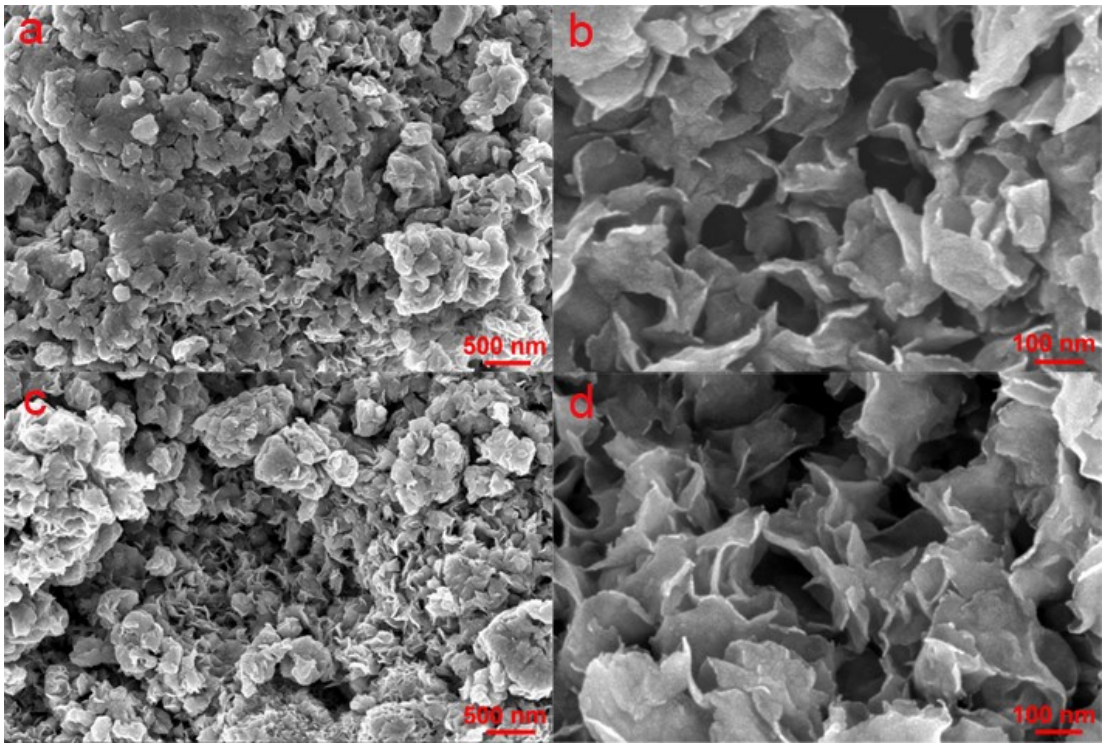

Fig. S1 SEM images of (a, b) SP-MoS_2-0.25 and (c, d) SP-MoS_2-0.75.

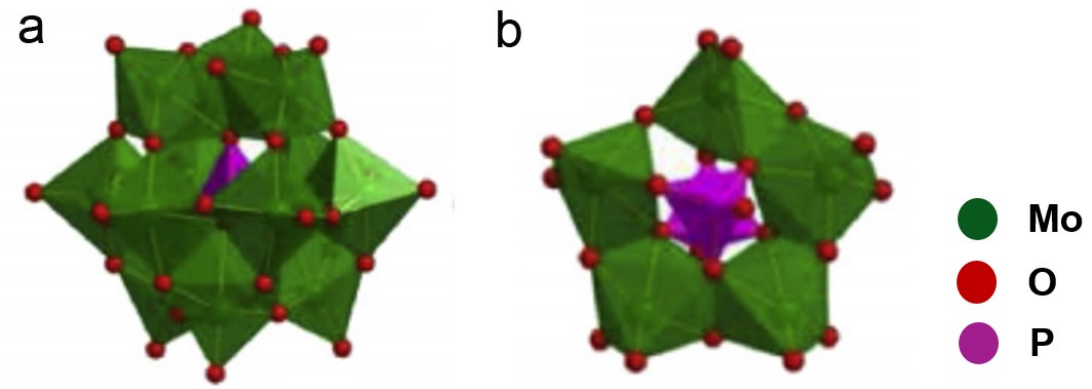

Fig. S2 Schematic illustration of PMo_{12} clusters.[6] (a) Keggin type, and (b) Strandberg type.

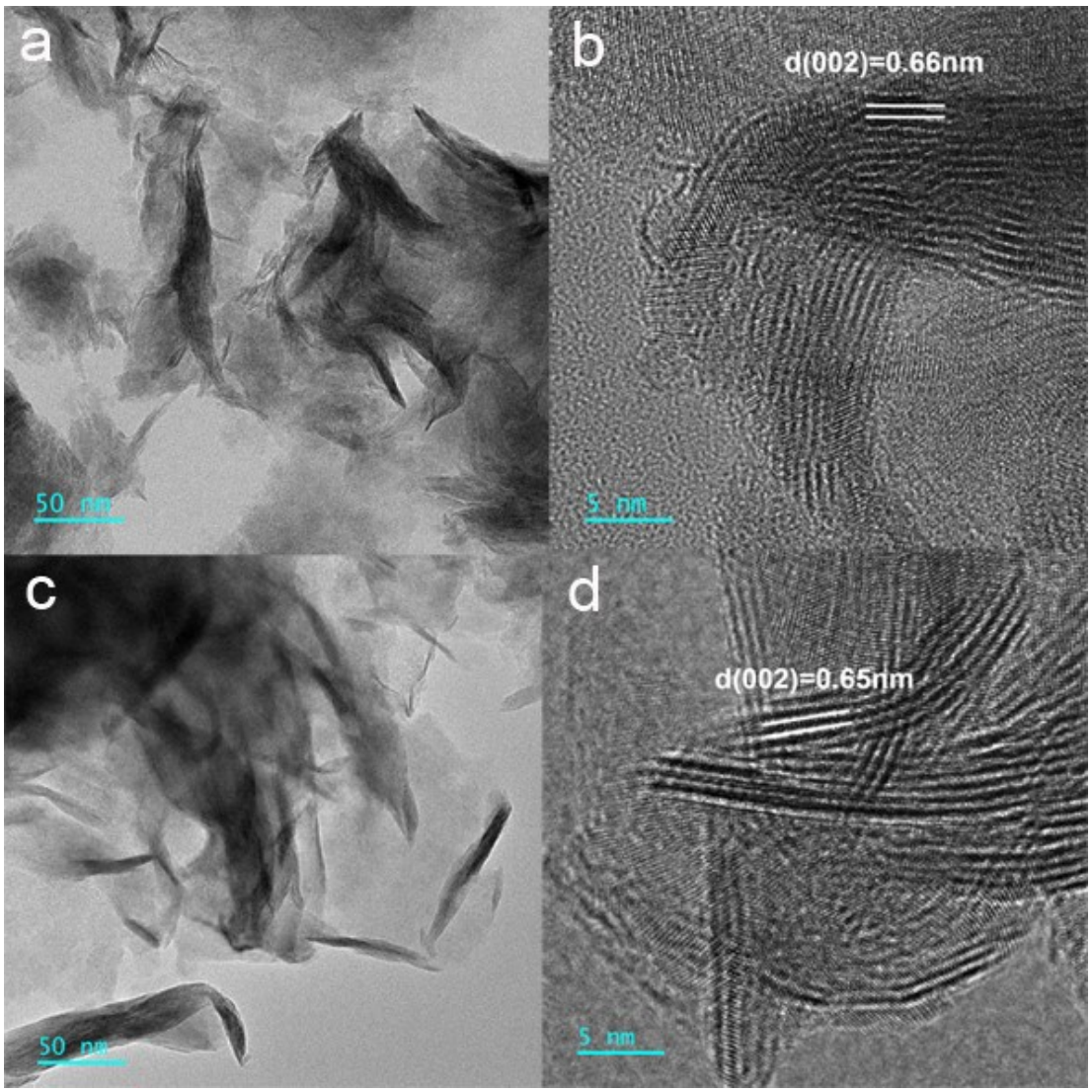

Fig. S3 TEM images of (a, b) P-MoS_2 and (c, d) MoS_2.

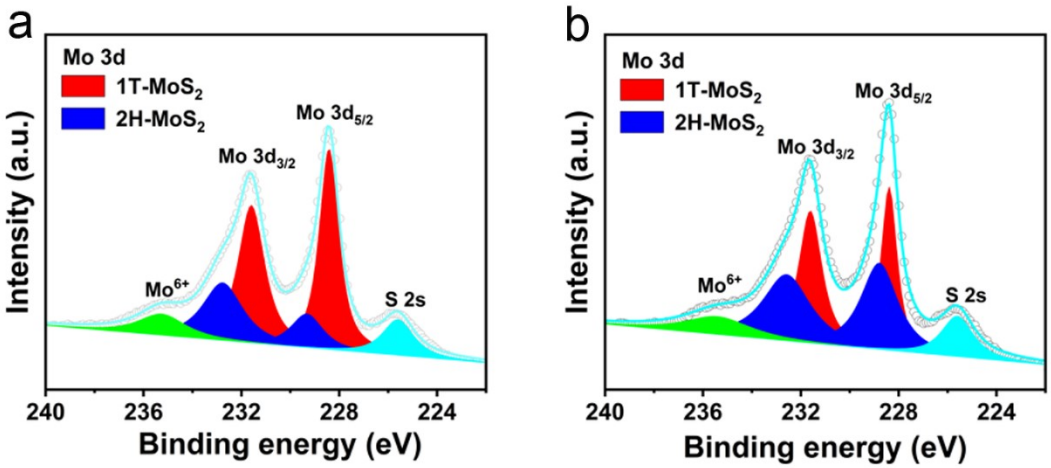

Fig. S4 The high-resolution Mo 3d XPS spectrum of P-MoS_2 (a) and MoS_2 (b).

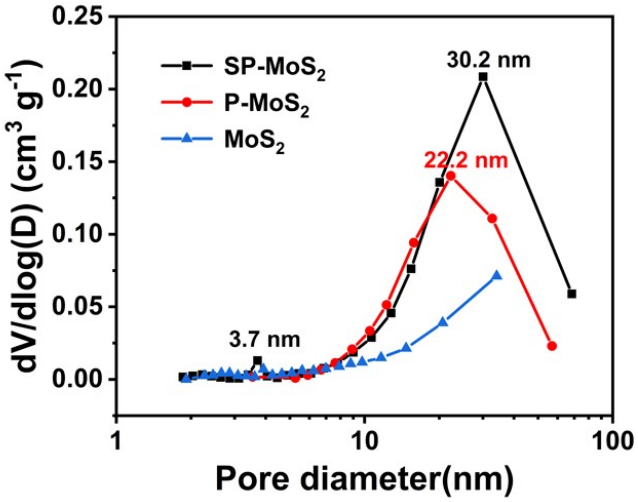

Fig. S5 Pore size distribution curves of MnP-MoS_2, P-MoS_2, and MoS_2.

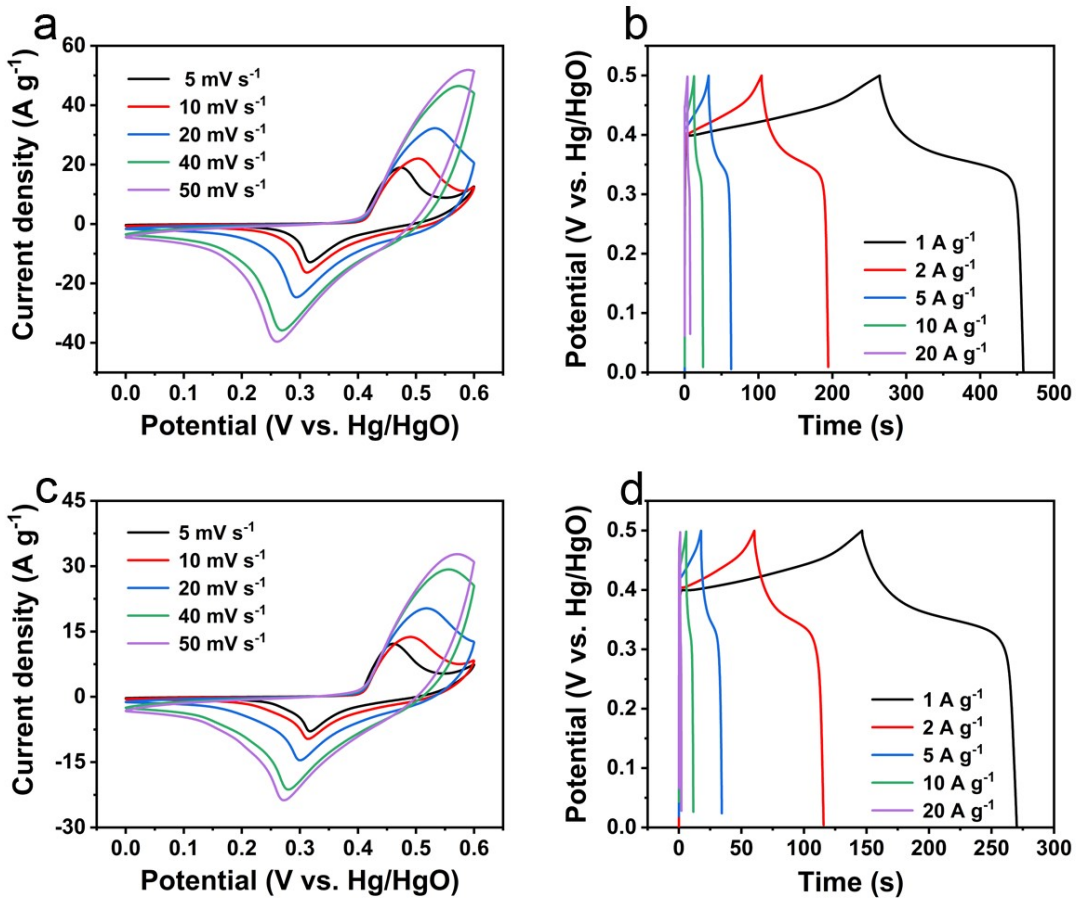

Fig. S6 Electrochemical performance of P-MoS_2 and MoS_2 in three-electrode system. CV curves at different scan rates: (a) P-MoS_2 and (c) MoS_2; GCD curves at different current densities: (b) P-MoS_2 and (d) MoS_2.

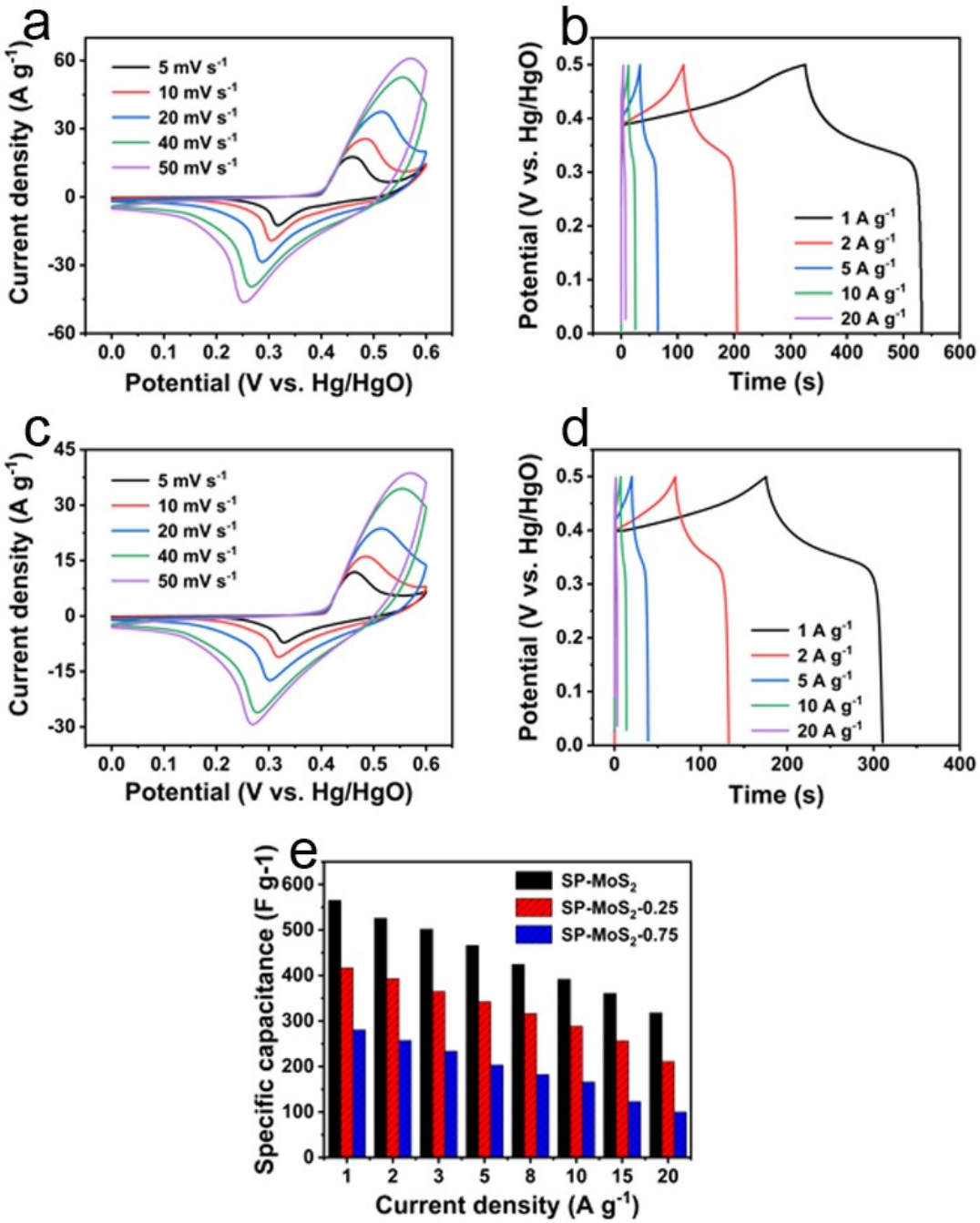

Fig. S7 (a) CV and (b) GCD curves of SP-MoS_2-0.25. (c) CV and (d) GCD curves of SP-MoS_2-0.75. (e) Specific capacitance versus current density curves of SP-MoS_2, SP-MoS_2-0.25 and SP-MoS_2-0.75.

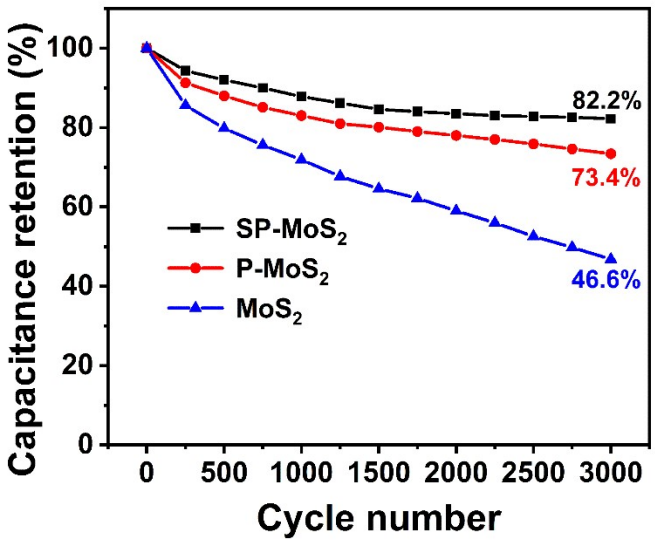

Fig. S8 Cycling stability of SP-MoS_2, P-MoS_2 and MoS_2 after 3000 cycles at a current density of 10 A g^{-1}.

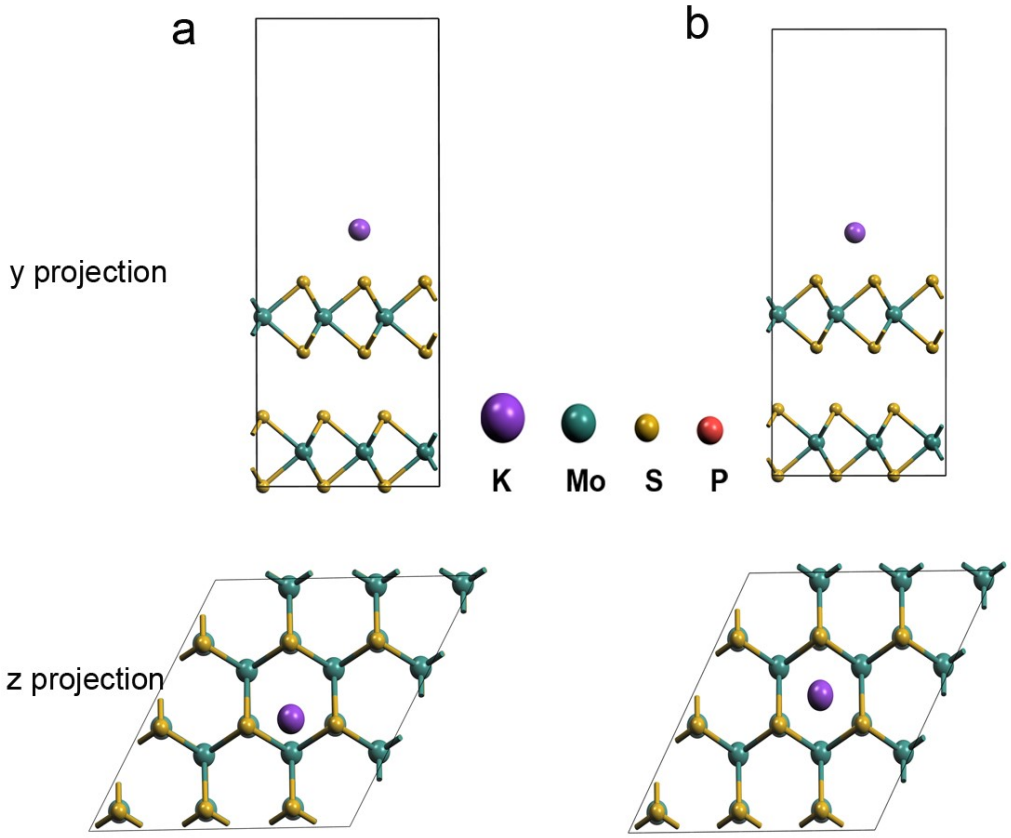

Fig. S9 The optimized K adsorption configuration on MoS_2 bilayer. (a) TopS site. (b) Hollow site.

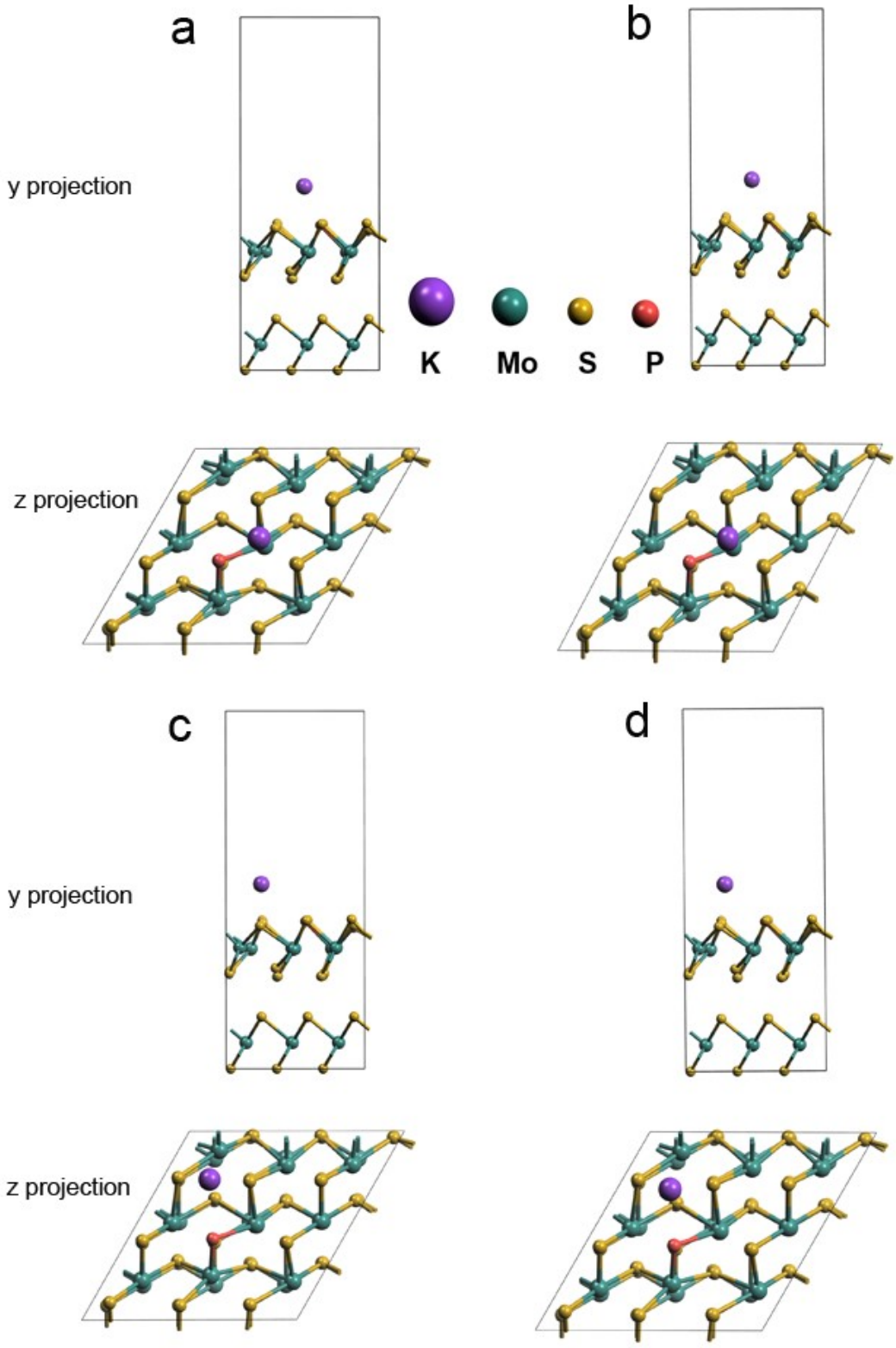

Fig. S10 The optimized K adsorption configuration on P-MoS_2 bilayer. (a) TopMo site. (b) TopS site. (c) TopP site. (d) Bridge site.

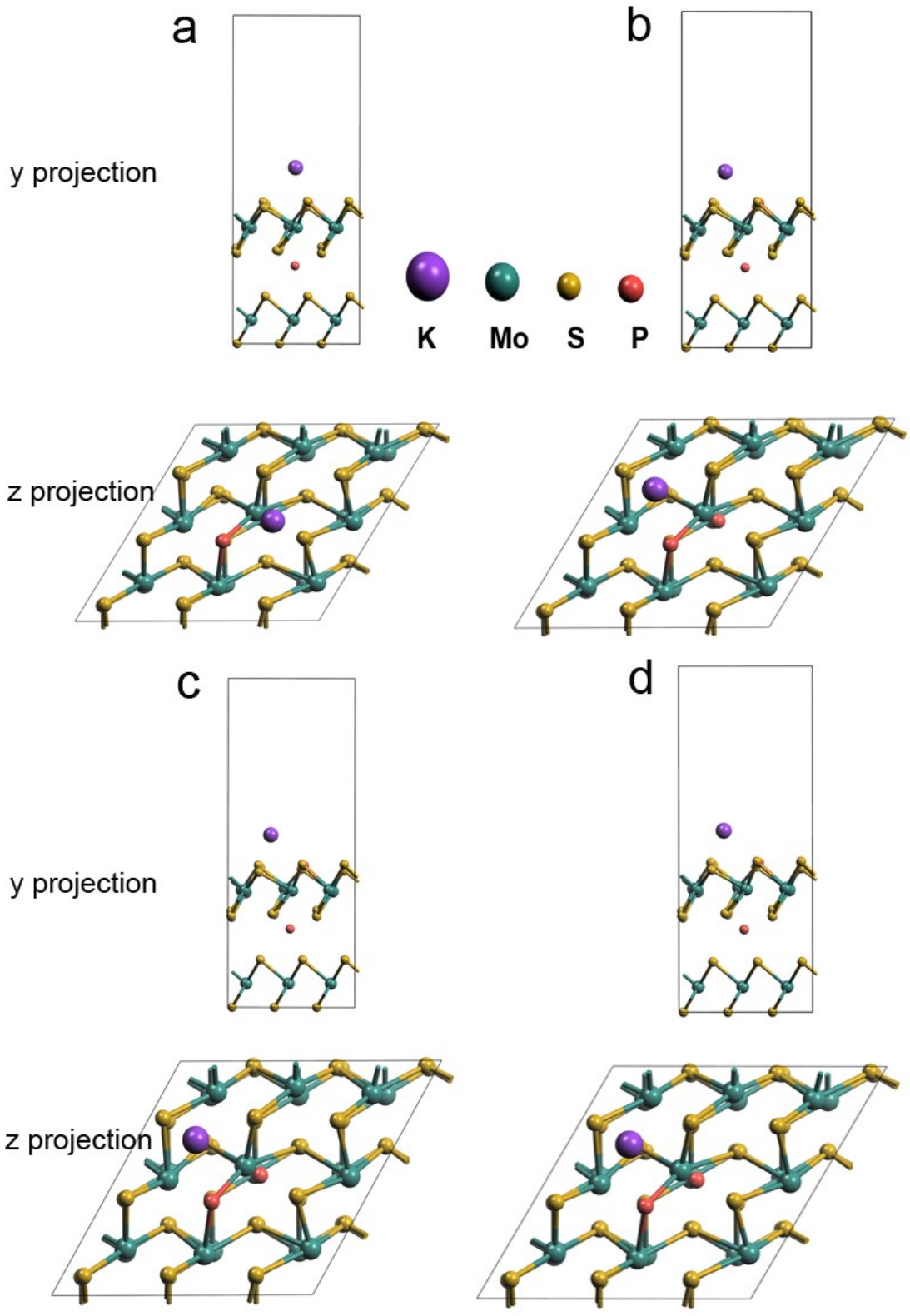

Fig. S11 The optimized K adsorption configuration on SP-MoS_2 bilayer. (a) TopMo site. (b) TopS site. (c) TopP site. (d) Bridge site.

Table S1 Comparative electrochemical performances (specific capacitance, rate capability and cycling stability) of MoS_2-based electrodes in neutral, acidic and alkaline electrolyte in the literature reports with our work.

Electrode material	Electrolyte	Specific capacitance	Rate capability	Cycling stability
LE-MoS_2 nanorods[7]	1 M Na_2SO_4	231 F g^{-1} at 1 A g^{-1}	~155 F g^{-1} at 10 A g^{-1}	76.6 % after 1000 cycles
E-MoS_2 microflowers[8]	1 M Na_2SO_4	246.8 F g^{-1} at 0.5 A g^{-1}	125.0 F g^{-1} at 5 A g^{-1}	70 % after 3000 cycles
MoS_2/NCQDs[9]	1 M Na_2SO_4	379.5 F g^{-1} at 0.5 A g^{-1}	269.7 F g^{-1} at 10 A g^{-1}	82 % after 5000 cycles
MoS_{2-x} nanosheets[10]	1 M Na_2SO_4	170.2 F g^{-1} at 0.5 A g^{-1}	91.8 F g^{-1} at 5 A g^{-1}	87.1 % after 5000 cycles
MoS_2/NCQDs[9]	1 M Na_2SO_4	379.5 F g^{-1} at 0.5 A g^{-1}	269.7 F g^{-1} at 10 A g^{-1}	82 % after 5000 cycles
MoS_2(Synergism)[11]	1 M Na_2SO_4	392 F g^{-1} at 1 A g^{-1}	~200 F g^{-1} at 10 A g^{-1}	87.1 % after 5000 cycles
A-MoS_2[12]	1 M Na_2SO_4	178 F g^{-1} at 1 A g^{-1}	118 F g^{-1} at 5 A g^{-1}	86 % after 5000 cycles
1T/2H-O-MoS_2@GF[13]	1 M Na_2SO_4	280F g^{-1} at 1 A g^{-1}	96 F g^{-1} at 20 A g^{-1}	88 % after 10000 cycles
N-doped 1T/2H MoS_2[14]	0.5 M H_2SO_4	410 F g^{-1} at 1 A g^{-1}	197 F g^{-1} at 20 A g^{-1}	80.9 % after 10000 cycles
Nitrogen-doped reduced graphene oxide/MoS_2[15]	1 M KOH	539.5 F g^{-1} at 1 A g^{-1}	160 F g^{-1} at 10 A g^{-1}	96.5 % after 20000 cycles
HDD-MoS_2[16]	1 M KOH	379 F g^{-1} at 1 A g^{-1}	227.4 F g^{-1} at 10 A g^{-1}	92 % after 3000 cycles
MnP-MoS_2[17]	2 M KOH	432.3 F g^{-1} at 1 A g^{-1}	241 F g^{-1} at 20 A g^{-1}	86.2 % after 2000 cycles
Co-decorated MoS_2 nanosheets[18]	2 M KOH	510 F g^{-1} at 1 A g^{-1}	400 F g^{-1} at 10 A g^{-1}	77.4 % after 5000 cycles
Sr-doped MoS_2[19]	3 M KOH	489.75 F g^{-1} at 1 A g^{-1}	~310 F g^{-1} at 10 A g^{-1}	62.5 % after 2000 cycles
MoS_2/N-CNTs[20]	6 M KOH	225 F g^{-1} at 1 A g^{-1}	90 F g^{-1} at 5 A g^{-1}	89 % after 10000 cycles
Cu doped MoS_2[21]	6 M KOH	353 F g^{-1} at 1 A g^{-1}	267 F g^{-1} at 10 A g^{-1}	94 % after 5000 cycles
SP-MoS_2 (Our work)	***2 M KOH***	***564.8 F g^{-1} at 1 A g^{-1}***	***391.5 F g^{-1} at 10 A g^{-1} 318.0 F g^{-1} at 20 A g^{-1}***	***76.5% after 3000 cycles***

Table S2 The adsorption energy of K^+ at different absorption sites on MoS_2, P-MoS_2 and SP-MoS_2 bilayers.

Sample	Absorption site	Adsorption energy (eV)
MoS_2	TopMo	-2.157
	TopS	-2.118
	Hollow	-2.149
P-MoS_2	TopMo	-3.426
	TopS	-3.426
	Hollow	-3.733
	TopP	-3.551
	Bridge	-3.547
SP-MoS_2	TopMo	-3.411
	TopS	-3.693
	Hollow	-3.693
	TopP	-3.692
	Bridge	-3.693

References

1 V. Milman, B. Winkler, J. A. White, C. J. Pickard, M. C. Payne, E. V. Akhmatskaya and R. H. Nobes, *Int. J. Quantum Chem.*, 2000, **77**, 895-910.

2 J. P. Perdew, A. Ruzsinszky, G. I. Csonka, O. A. Vydrov, G. E. Scuseria, L. A. Constantin, X. Zhou and K. Burke, *Phys. Rev. Lett.*, 2008, **100**, 136406.

3 J. P. Perdew, K. Burke and M. Ernzerhof, *Phys. Rev. Lett.*, 1996, **77**, 3865–3868.

4 W. Jia, H. Wu, Y. Zheng, Z. Liu, G. Cai, J. Wen, G. Hu, T. Tang, X. Li, L. Jiang, Z. Wang, M. Li and H. Huang, *ACS Appl. Energy Mater.*, 2023, **6**, 2570-2581.

5 X. Liao, R. Lu, L. Xia, Q. Liu, H. Wang, K. Zhao, Z. Wang and Y. Zhao, *Energy Environ. Mater.*, 2021, **5**, 157-185.

6 J. Luo, C. Xiao, Y. Xiao, X. Lin, Y. Chen, B. Gao and B. Lin, *Int. J. Hydrogen Energy*, 2020, **45**, 12318-12330.

7 H. Xiao, S. Wang, S. Zhang, Y. Wang, Q. Xu, W. Hu, Y. Zhou, Z. Wang, C. An and J. Zhang, *Mater. Chem. Phys.*, 2017, **192**, 100-107.

8 J. Wang, X. Zheng, Y. Dong, L. Chen, L. Chen and W. He, *Dalton Trans.*, 2023, **52**, 4537-4547.

9 K. Yang, Z. Luo, D. Shu, F. Yi, Z. Zhu and A. Gao, *J. Electroanal. Chem.*, 2022, **908**, 116093.

10 H. Wang, X. Xu and A. Neville, *RSC Adv.*, 2021, **11**, 26273-26283.

11 H. Li, H. Li, Z. Wu, L. Zhu, C. Li, S. Lin, X. Zhu and Y. Sun, *J. Mater. Sci. Technol.*, 2022, **123**, 34-40.

12 X. Sun, Y. a. Pang, S. Li, Y. Yu, X. Ding, L. Wang and Q. Zhang, *Ceram. Int.*, 2022, **48**, 21317-21326.

13 S. Lee, J. Hwang, D. Kim and H. Ahn, *Chem. Eng. J.*, 2021, **419**, 129701.

14 K. Le, X. Zhang, Q. Zhao, Y. Liu, P. Yi, S. Xu and W. Liu, *ACS Appl. Mater. Interfaces*, 2021, **13**, 44427-44439.

15 S. W. Bokhari, A. V. Ellis, M. Uceda, S. Wei, M. Pope, S. Zhu, W. Gao and P. C. Sherrell, *J. Energy Storage*, 2022, **56**, 105935.

16 N. Joseph, P. Muhammed Shafi and A. Chandra Bose, *New J. Chem.*, 2018, **42**,

12082-12090.

17 Y. Li, X. Wang, J. Meng, M. Song, M. Jiao, Q. Qin and L. Mi, *New J. Chem.*, 2023, **47**, 15143-15150.

18 A. Sun, L. Xie, D. Wang and Z. Wu, *Ceram. International*, 2018, **44**, 13434-13438.

19 T. K. Selvam, K. Silambarasan, K. Prakash, J. Archana, S. Harish, A. M. F. Benial and T. Mathavan, *J Mater Sci: Mater. Electron.*, 2023, **34**, 345.

20 W. Liu, W. Zhang, S. Zuo, C. Yao and X. Li, *J. Mater. Sci.: Mater. Electron.*, 2021, **32**, 27184-27197.

21 D. Vikraman, S. Hussain, K. Karuppasamy, A. Kathalingam, E.-B. Jo, A. Sanmugam, J. Jung and H.-S. Kim, *J. Alloys Compd.*, 2022, **893**, 162271.